Well-defined Pt surfaces for the Ethanol Oxidation Reaction

Dr. Rubén Rizo[1*], Dr. S. Pérez-Rodríguez[2], Dr. Gonzalo Garcia[1]

1 Instituto de Materiales y Nanotecnología, Departamento de Química, Universidad de La Laguna, PO Box 456, 38200, La Laguna, Santa Cruz de Tenerife, Spain
2 University of Southampton, University Road, Highfield, Southampton SO17 1BJ, UK

* Corresponding author: rizo@fhi-berlin.mpg.de

Abstract

Direct ethanol fuel cells are a promising technology for clean energy production. The ethanol oxidation reaction is surface-sensitive and hence, the study of single-crystal electrodes provides fundamental knowledge on the different activity of the metal crystal planes. However, for practical applications, metal nanoparticles dispersed on a porous support are generally used to enhance the efficiency and to reduce the catalyst cost. Although some research has been devoted to the development of shape-controlled nanoparticles, the finding of an efficient, cost-effective and easily scaled-up catalytic system remains a challenge. Furthermore, the use of suitable support with a well-defined nanoarchitecture is essential for the control of the catalyst reactivity.

In this review, a general overview of the performance of single-crystal electrodes and un-supported/supported shape-controlled nanoparticles, for EOR is presented, paying special attention to Pt surfaces. Finally, the major challenges and directions for future research are also discussed to guide the design of efficient shape-controlled catalysts for the EOR.

Keyboards: Catalyst support, DEFCs, ethanol electrooxidation, nanoparticles, single crystals

Table of content
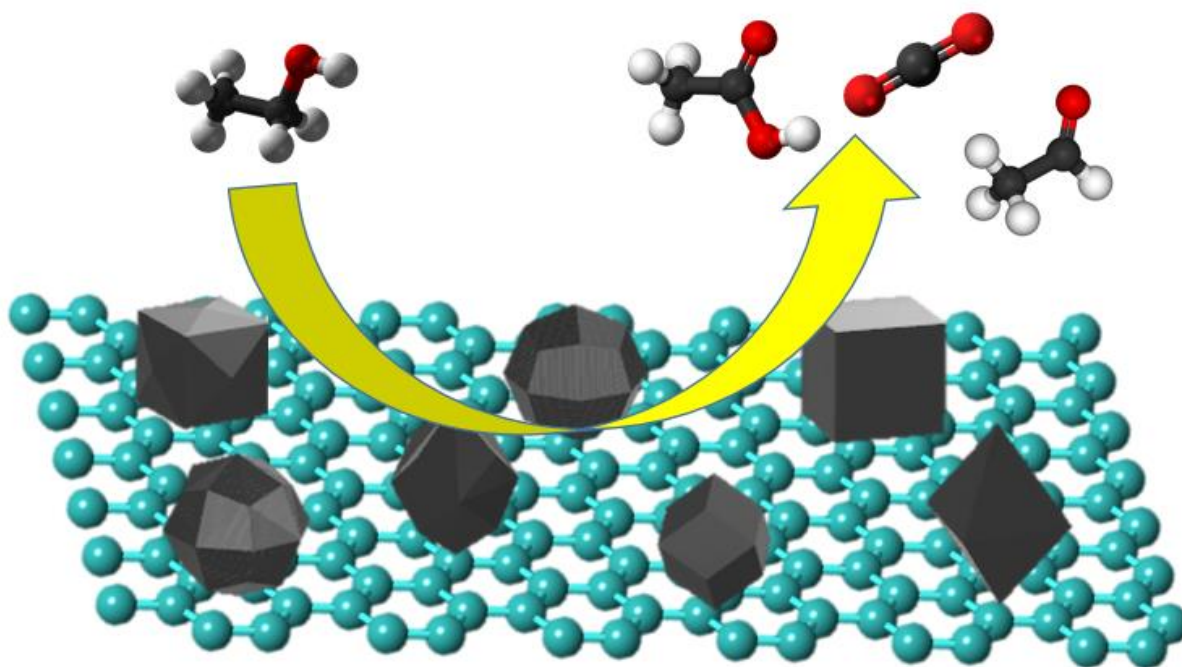
Shape matters: Ethanol oxidation reaction is a sensitive-structure reaction, which makes essential controlling the shape of the catalytic metal nanoparticles and the morphology of the catalyst support to enhance the efficiency and reduce the cost of the catalyst. This review summarizes the most relevant studies on Pt single-crystal electrodes studies and un-supported/supported shape-controlled nanoparticles for ethanol oxidation reaction, including a discussion about the major challenges and directions for future research to guide the design of efficient shape-controlled catalysts for this reaction.

Introduction

Direct alcohol fuel cells (DAFCs) have emerged as a promising clean alternative to the use of contaminant fossil fuels systems to fulfill the energy demands. Ethanol, in particular, is the most interesting molecule to be used in such systems since it is the major renewable bio-fuel and less toxic than other alcohols as methanol. The oxidation of ethanol in these devices requires the use of a metal catalyst, normally composed by nanoparticles (NPs), well dispersed on a high surface area material. The better the dispersion and the smaller the NPs size, leads to a higher metal "utilization" (ratio of atoms to bulk) and a cheaper catalyst[1,2]. Among the different metal candidates, Pt has been postulated as the most efficient metal for the ethanol oxidation reaction (EOR) in DEFCs[3,4].

Different classic electrochemical methods, as cyclic voltammetry (CV) and chronoamperometry and other spectroelectrochemical methods, such as, *in situ* Fourier transform infrared (FTIR) or differential electrochemical mass spectrometry (DEMS), have been widely employed for the elucidation of different mechanistic steps and for clarifying the presence of possible intermediates and products during the EOR on Pt surfaces. By compilation of all these studies, we recently provided a global mechanism for the EOR on Pt surfaces in acidic media (scheme 1)[5].
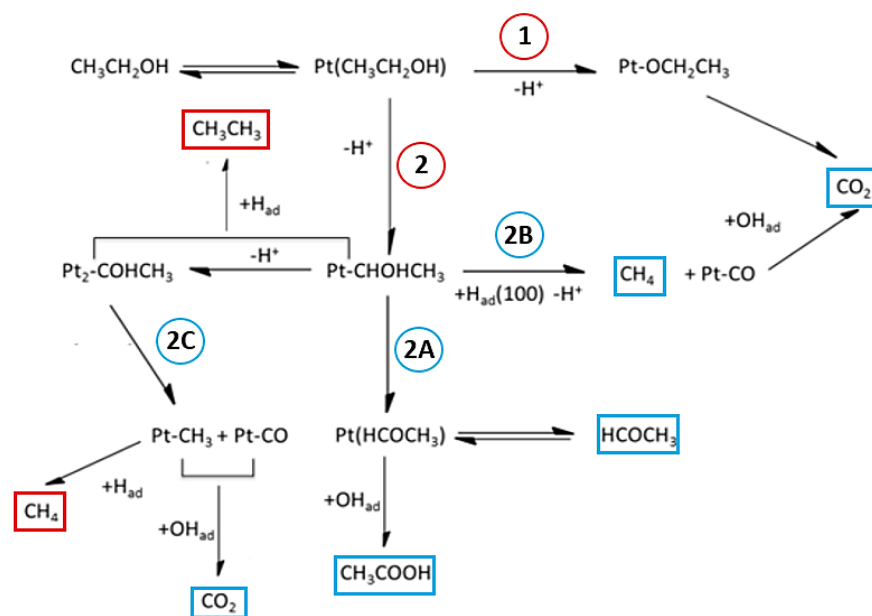
Scheme 1. Reaction mechanism of the ethanol oxidation on Pt electrode in acidic media. Species inside the red and light blue boxes are produced during the backward and forward scans, respectively. Modified with permission from ref 5. Copyright 2016 Elsevier

The full oxidation of ethanol to carbon dioxide has a thermodynamic potential of 0.08 V vs SHE. However, it involves several steps such as adsorption, C-C bond scission, dehydrogenation, electrooxidation of adsorbed intermediates (e.g. CO and CH_3 species) and formation of soluble species (e.g. acetaldehyde and acetic acid) that strongly modify the reaction rate as well as the conversion efficiency for CO_2 formation. At fuel cell operation conditions, ethanol conversion efficiency for CO_2 formation is lower than 6 %[5,6] Therefore, main investigations are devoted to increase the alcohol intermediate pathway (2 in Scheme 1), as well as to rise the C-C bond breaking and the CO tolerance (2B and 2C in Scheme 1). The initial electroadsorption step of ethanol at small overpotentials (E < 0.4 V vs SHE) dictate the reaction pathway:

➢ Formation of stable adsorbed ethoxy species (1 in scheme 1). This species may oxidize at high overpotentials (E > 0.6 V).

➢ Formation of alcohol intermediate (2 in scheme 1). C-C bond breaking may happen producing methane and adsorbed species (2B and 2C in Scheme 1), which will oxidize to CO_2 at high overpotentials (E > 0.6 V). 2B and 2C pathways are favored at open surface structures (Pt(100) and Pt(110)), as well as at surfaces with high density of low coordinated sites (steps, kinks and defect sites).

At higher potentials than 0.4 V vs SHE, ethanol dehydrogenates to produce acetaldehyde and oxidizes to form acetic acid through the alcohol intermediate route (2A in Scheme 1). These products are not desired since strongly decrease the overall fuel cell efficiency, although they are actually the main responsible for more than 60 % of the delivered current[7–9].

As can be seen, many adsorbed intermediates on Pt are involved in the mechanism for the EOR. These intermediates interact with the surface, modifying the energetic levels of their molecular orbitals, and hence, varying the energies of activation and enabling new reaction routes. Thus, it is important to evaluate in depth the influence of the morphology of the Pt surface structure in the mechanism for the EOR from a fundamental point of view, by means of the use of Pt single crystals with well-defined surface geometry. The geometric orientation of these face centered cubic (fcc) Pt single crystal surfaces are usually named by their Miller indices and can be depicted in a stereographic triangle as shown in Figure 1. At the vertexes of the triangle are disposed the three basal planes, (111), (100) and (110) with a single type of symmetry, while at the edges of the triangle stepped surfaces can be found, consisting in ideal structures composed of flat terraces separated by monatomic steps.
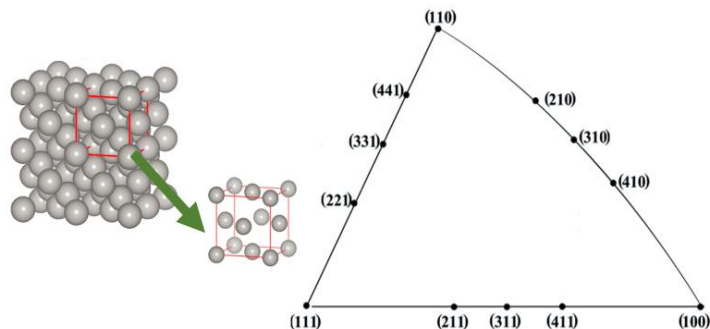
Figure 1. Schematic 3D representation of the fcc structure of Pt and the stereographic triangle containing Miller index of different possible Pt planes.

The study of EOR on stepped surfaces makes possible to study the influence of the defects on the ideal flat surfaces. These steps have a lower index of coordination and are generally more reactive than the atoms on a surface without defects. The reason for the greater activity in the defects is the electronic alteration in these sites since the local "d" band narrows reaching energies close to the Fermi level. This results in higher adsorption energies for many adsorbates at the steps, and consequently, according to the Bronsted-Polanyi relationship[10], lower energies of activation in the dissociation reactions of the adsorbed species on these sites.

Nevertheless, from a practical point of view the use of single crystals electrodes in a fuel cell system is not realistic. The use of metallic nanoparticles (NPs) well dispersed on an appropriate is crucial to minimize the metal "utilization" (ratio surface area/volume of the metal), which leads to a reduction of the catalyst cost and an increase of the catalytic efficiency. To fulfill this object, many authors have focused on the synthesis and the study of shape-controlled nanosized metal particles with predominant domain of the facet of interest[2].

Furthermore, the use of an optimum material for supporting these NPs is also essential. In order to increase the electrochemical active surface of the catalyst and to reach a good dispersion of the NPs, catalyst supports with a high specific surface areas have been widely employed in DEFCs. In addition to high surface area, electrical conductivity, an accessible porosity, corrosion resistance and roles as promoter or co-catalyst are also crucial properties for an optimum choice of the catalyst support which could be fine-tuned by controlling the nanostructure of the material[1,11–14].

The purpose of this review is to provide a better insight into the most relevant fundamental works (single crystals) and applied studies on shape controlled surfaces (catalyst and catalyst support) used as anodes in DEFCs, in the light of the latest advances on this field. Special attention has been paid to Pt

surfaces due to its high activity for ethanol oxidation. This work offers also a general vision on future needs in order to guide subsequent research lines.

1 Single-crystals studies

The knowledge acquired from metal single crystals studies is not only of critical importance for the understanding of the relationships between surface structure and reactivity, but also should be employed as a baseline for those studies dealing with the surface structure influence on the electrocatalytic properties of metal NPs. As mentioned in the introduction, Pt is the most active metal for the EOR and consequently, most of the studies on single crystals have been carried out on this metal. The first studies on Pt single crystals date from the 60s and 70s of the last century[15–18]. However, it was not until the beginning of the 1980s when the flame-annealing treatment was developed as a new method for the preparation of these electrodes[19]. This procedure allowed, for the first time, to obtain ordered and clean surfaces with a high reproducibility of the electrochemical results in a simple way. Afterward, consecutive studies have been performed on the study of many electrochemical reactions of interest by using Pt single crystals. In particular, the influence of the surface structure of Pt single crystals for EOR has been examined by using cyclic voltammetry and chronoamperometry techniques to study the reactivity of the system, and *in situ* Fourier transform infrared spectroscopy (FTIRS) to find the intermediates and final species formed during the ethanol oxidation on Pt basal plane. Interestingly, Feliu et al. found that the reactivity of Pt surfaces for EOR is greatly affected by the pH of the electrolyte. Whereas in acid media (pH = 1) the peak currents increase in the order of Pt(111) < Pt(110) < Pt(100) (Figure 3a)[20], in alkaline electrolytes (pH = 13) higher current intensities were measured and the peak currents were found following the sequence Pt(100) <Pt(110) <Pt(111) (Figure 3b)[21].
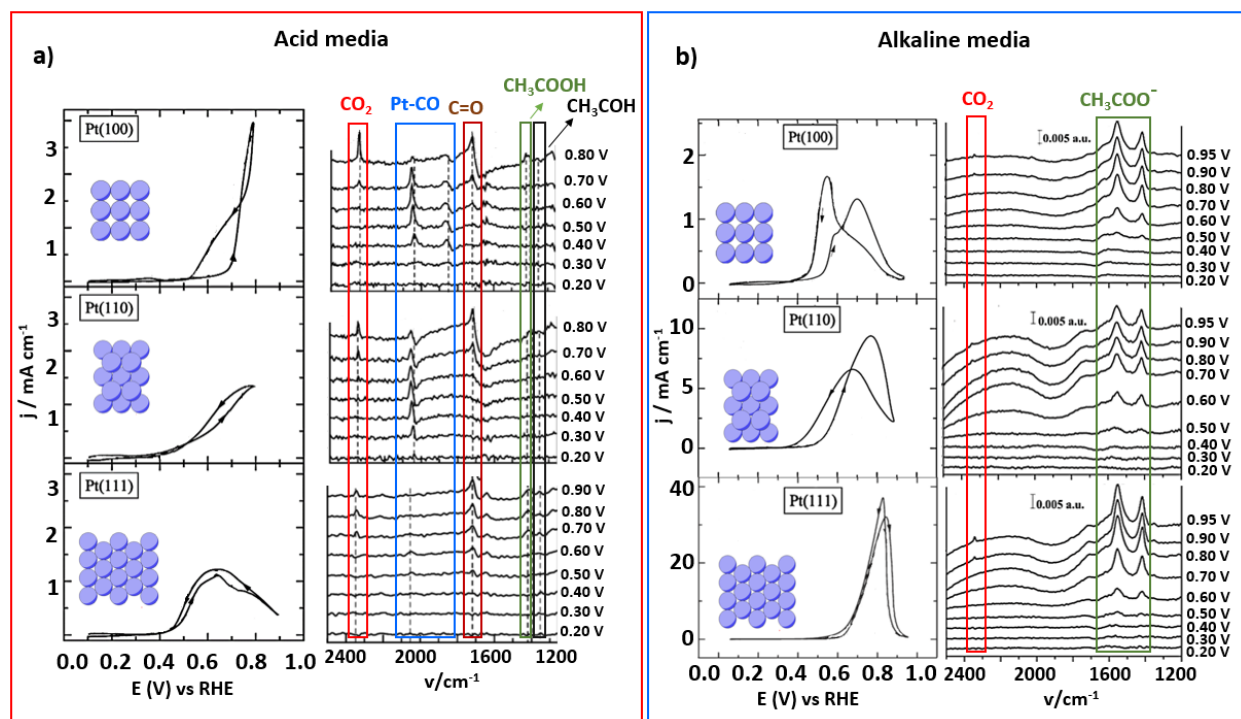
Figure 2. Cyclic voltammograms at 50 mV/s (left) and FTIR spectra at different potentials (right) for Pt(111), Pt (110), and Pt(100) electrodes in (a) 0.1 M HClO$_4$ + 0.2 M EtOH and (b) 0.2 M EtOH + 0.1 M NaOH. Reproduced with permission from ref 20. Copyright 2009 Royal Society of Chemistry (a), and from ref 21. Copyright 2014 Royal Society of Chemistry (b).

FTIR experiments carried out in both electrolytes also showed differences in the mechanism depending on the surface structure or the pH of the solution (Figure 2a-b). FTIR spectra in acidic medium demonstrated that EOR occurs almost exclusively following the path of incomplete oxidation on Pt (111), without rupture of the C-C bond and with almost no CO$_2$ and CO$_{ad}$ formation (A2 in Scheme 1). In contrast, Pt (100) deactivates fast at small overpotentials due to adsorbed CO (CO$_{ads}$) formation that strongly poison the electrodes (2B and 2C in Scheme 1). However, these CO adsorbates are oxidized between 0.65 and 0.80 V vs. RHE, releasing Pt active sites, and hence, allowing the ethanol oxidation to acetaldehyde and acetic acid at higher values than those potentials (2A in Scheme 1). On the other hand, the Pt (110) surface shows the highest catalytic activity for the breaking of the C-C bond, leading to the formation of CO$_{ads}$, both coming from ethanol and acetaldehyde, at a high rate at any potential (2C in Scheme 1). This is consistent with density functional theory calculations (DFT), which demonstrated that surface planes with less-coordinated surface atoms are generally more active for bond breaking (coordination number of (111), (100) and (110) planes is 9, 8 and 7, respectively)[22]. However, in alkaline media, the selectivity for CO$_2$ production is much lower but the surfaces deactivate faster due to the acetaldehyde formation, which readily polymerizes and strongly adsorbs on the Pt surface[21]. This blocking mechanism was found to follow the

7

order Pt(111) > Pt(110) > Pt(100). studies concluded that low-coordinated surface sites can facilitate α-dehydrogenations toward CO_2 (1 in Scheme 1) and in contrast, the formation of acetic acid is less favored on such surface structures. The lower acetic acid formation on low-coordinated surfaces is largely determined by the potential energy surface of OH on surfaces. Energy barrier height calculations suggested that lower-coordinated surfaces tend to bond OH more strongly at bridge sites than at atop sites. This extra energy cost, due to the corrugation of the OH potential energy surface, thus decreases OH activity In general, DFT, since OH must be activated to an atop site to free its 2p-states before reacting with other species [22].

Furthermore, anions and cations play an important role in electrocatalysis at low and high pH, respectively [23,24]. Sulfate and phosphate species adsorb stronger on Pt surfaces than perchlorate species and therefore higher catalytic activity toward the EOR in perchloric acid solution is observed. On the other hand, at high pH metal cation species change the adsorption potential of hydroxide species at open surface, which are necessary to oxidize and remove the main catalyst poison (CO) from the catalyst surface[23,24]. The role of alkali cations (Li^+, Na^+, K^+, Cs^+, and Be^{2+}) on the oxidative stripping of carbon monoxide from stepped Pt single-crystal electrodes in alkaline media has been reported [25]. Main results suggested that Li^+ and Be^{2+} cations markedly affect the adsorption of OH (at both on steps and on terraces) and thereby have a significant promoting effect on the CO oxidation reaction [25].

Beyond the ideal flat Pt structures, the presence of defects on the surface greatly influences the reactivity of the electrode and great enhancement for C-C bond breaking and CO removal was reported[21,23,26,27]. In this sense, the role of steps in the electroactivity and mechanism towards the EOR have been studied by employing Pt stepped surfaces containing (111) terraces with (100) monoatomic steps and stepped Pt surfaces having (111) terraces with (110) monoatomic steps[21,26]. These series surfaces are denoted as Pt(S)[n(111)x(100)]=Pt(n+1,n-1,n-1) for the surfaces with (100) steps and Pt(S)[(n-1)(111)x(110)]=Pt(n,n,n-2) for those with (110) steps, being n the number of rows in the (111) terrace:

i) In acidic media, Colmati et al. revealed that the Pt (554) plane is the most electroactive electrode toward the oxidation of ethanol and that almost no significant enhancement is provided by the presence of (100) steps on (111) terrace (right panel of Figure 3a), whereas the activity increases with the presence of (110) steps (left panel of Figure 3a)[26]. FTIR experiments showed that at smaller potentials than 0.7 V, (110) steps favors the C-C bond breaking from ethanol, while at higher potentials than 0.7 V the (110) defects also promotes the oxidation of ethanol to form acetaldehyde and acetic acid.

ii) On the other hand, Buso et al. proved that in alkaline media the presence of (100) (right panel of Figure 3b) and/or (110) (left panel of Figure 3b) steps on (111) terraces does not improve peak current densities

(Figure 3b)[21]. However, the onset potential for the ethanol oxidation shifted towards more negative potentials and the hysteresis between positive and negative scan directions increases. Interestingly, the surfaces with high step density, Pt(553) and Pt(533), showed significant currents in the negative scan direction up to 0.35 V vs RHE. Additionally, a larger current was observed for the (100) step in comparison to (110) step surfaces in the negative scan direction for comparable step densities. These results show a higher reactivity of (100) steps compared to (110) steps in alkaline media, conversely to the trend in acid media. Indeed, current transients recorded at 0.6 V vs RHE (Figure 3c) revealed a lower current decay for the series with (100) steps. On the other hand, a rise in the deactivation rate by increasing the (111) terrace length was also observed. The last was attributed to the lower catalytic activity toward the $CH_{x,ad}$ oxidation on (111) terrace in comparison to steps [28].
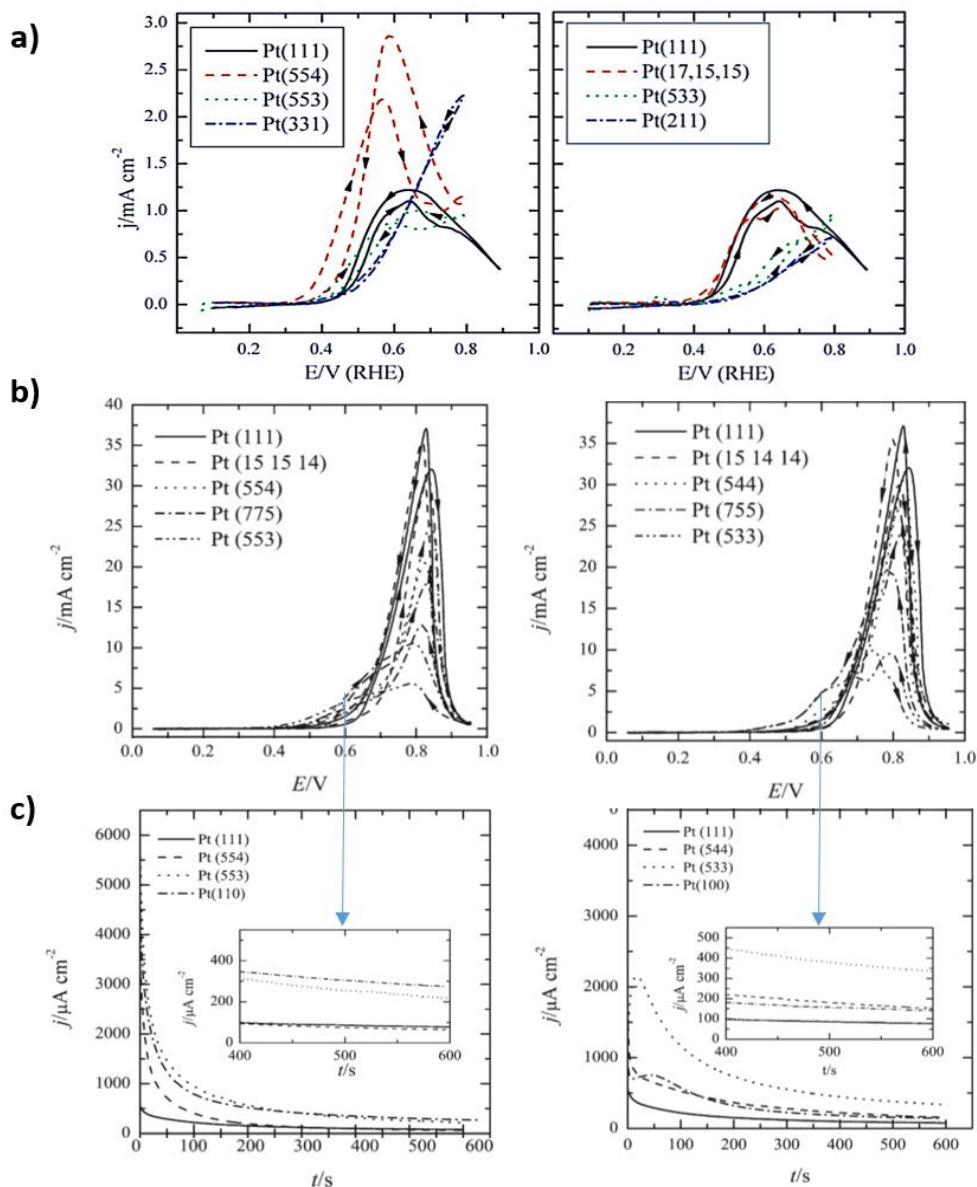
Figure 3. Cyclic voltammograms for EOR on stepped surfaces having (111) terraces with (110) monoatomic steps (left panel) or with (100) steps (right panel) monoatomic steps in (a) 0.1 M $HClO_4$ + 0.2 M EtOH and (b) in 0.1 M NaOH + 0.2 M EtOH. Scan rate 50 mVs^{-1}. (c) Chronoamperometric transients at 0.6 V for EOR on stepped surfaces having (111) terraces with (110) monoatomic steps (left panel) or with (100) steps (right panel) in 0.1 M NaOH + 0.2 M EtOH. Reproduced with permission from ref 26. Copyright 2009 Royal Society of Chemistry (a), and from ref 21. Copyright 2014 Royal Society of Chemistry (b, c).

A good alternative in the development of highly active electrocatalysts is the combination of different metals. Since Pt is the most active pure metal catalyst for EOR in acid media, most workers have quite reasonably approached electrocatalytic studies by Pt single crystals decoration with other metals. Metals like Sn, Ru and/or Os have been employed for the modification of Pt single crystal surfaces, exhibiting a general improvement in

terms of activity for the modified Pt surface [29–31]. This improvement has been mainly attributed to the oxophilicity of the adatom that activates the water at smaller overpotentials than pure Pt, allowing the oxidation of the ethanol molecule and poisoning intermediates (mainly CO_{ads}) at smaller overpotentials compared to bare Pt surface. Those works focused mainly on the effect of catalyst composition but unfortunately, almost no information about the structure influence and the presence of specific atomic ensemble on reactivity has been reported.

Despite some works have demonstrated that other platinum group metals (such as Rh or Pd) are active for the EOR in alkaline electrolytes (in the case of Pd exhibiting even a greater performance than Pt) [32,33], studies of the structure sensitive and the reaction mechanism involving single crystals of other any metal are scarce, however. In this regard, only one DFT study on the reaction mechanisms for EOR on Pd basal planes surfaces can be found in the literature [34]. In this study authors calculated the binding energies of ethanol interacting to Pd(100), Pd(110), and Pd(111) and the barrier energies of ethanol dehydrogenation on Pd(100), Pd(110), and Pd(111) and they concluded that the strong interaction between ethanol and the surface of palladium lead to the lowest barrier energies for ethanol dehydrogenation on Pd(100). The results demonstrated that the activity and selectivity of ethanol oxidation on Pd are highly structure-sensitive and proved that Pd(100) is the best surface for the dissociation of an ethanol molecule with a rather low energy barrier. In addition, in the presence of OH, a complete ethanol oxidation reaction is carried out on this surface.

2   Shape-controlled metal nanoparticles for EOR

Many synthesis methods have been described in the literature for the synthesis of shape-controlled NPs for the EOR. Here we will classify them into two main groups: i) methods that involve the reduction and growth of the metal precursor by applying potential (electrochemical methods); and ii) routes that employ a chemical compound to reduce the metal salt (chemical methods). Chemical methods are more popular because they are easily scaled up and offer an easier way to control the uniformity of the shaped NPs compared to electrochemical methods. However, most of these chemical methods require the use of organic solvents, surfactants or capping agents for controlling the growth of the NPs with a particle shape. These organic compounds may strongly attach on the surface of the catalyst with the consequent blocking of the metal active sites by spectator species. This effect, which is known as the "third-body effect" or "ensemble effect" was reported for the first time by Conway and coworkers [35]. Therefore, a surface cleanness of the catalyst after the chemical synthesis is essential as otherwise, organic molecules could block the catalyst surface and hinder the catalytic activity [36]. However, the removal of the surfactant without altering the initial surface structure of metal NPs is not always trivial. Nevertheless, some groups have also been developed chemical routes without the need of a surfactant. On the other hand, adsorbed

organic molecules on the catalyst surface may act as protecting agents under severe conditions, such as those founded in phosphoric acid fuel cells [37]. Additionally, the "ensemble effect" can be employed to drive a specific reaction, as usually demonstrated the group of Cuesta [38].

During the following two sections, we will review the most important works following both electrochemical and chemical methods for the synthesis of shaped NPs to be used as catalysts for the EOR.

2.1 Electrochemical synthesis

Only a few works can be found in the literature about electrochemical methods for the synthesis of shape-controlled NPs for the EOR. All of them have in common the growth of high-index noble pure metal NPs (Pt, Rh and Pd), tetrahexahedral (THH) NPs mainly[39–42], involving a two steps electrochemical process. In the first step, the growth of the crystal nucleus occurs. Crystal nucleus are the seed, which act as a template for the posterior shaped nanocrystals growth. This stage is controlled by a potential holding technique and/or an electrochemical square wave potential method (Figure 4 a-c). In general, the glassy carbon electrode, immersed in a solution containing the metallic precursor, is first hold at enough positive potentials to oxidize completely any adsorbate, leading to a clean surface. Subsequently, the potential is stepped to more negative values, at which the reduction of the metal precursor and the nucleation process can take place. This step is essential and the control of the upper and lower potential is crucial for an appropriate growth of the crystal nucleus. When the nucleation step is skipped, the products consist of mixed morphologies.
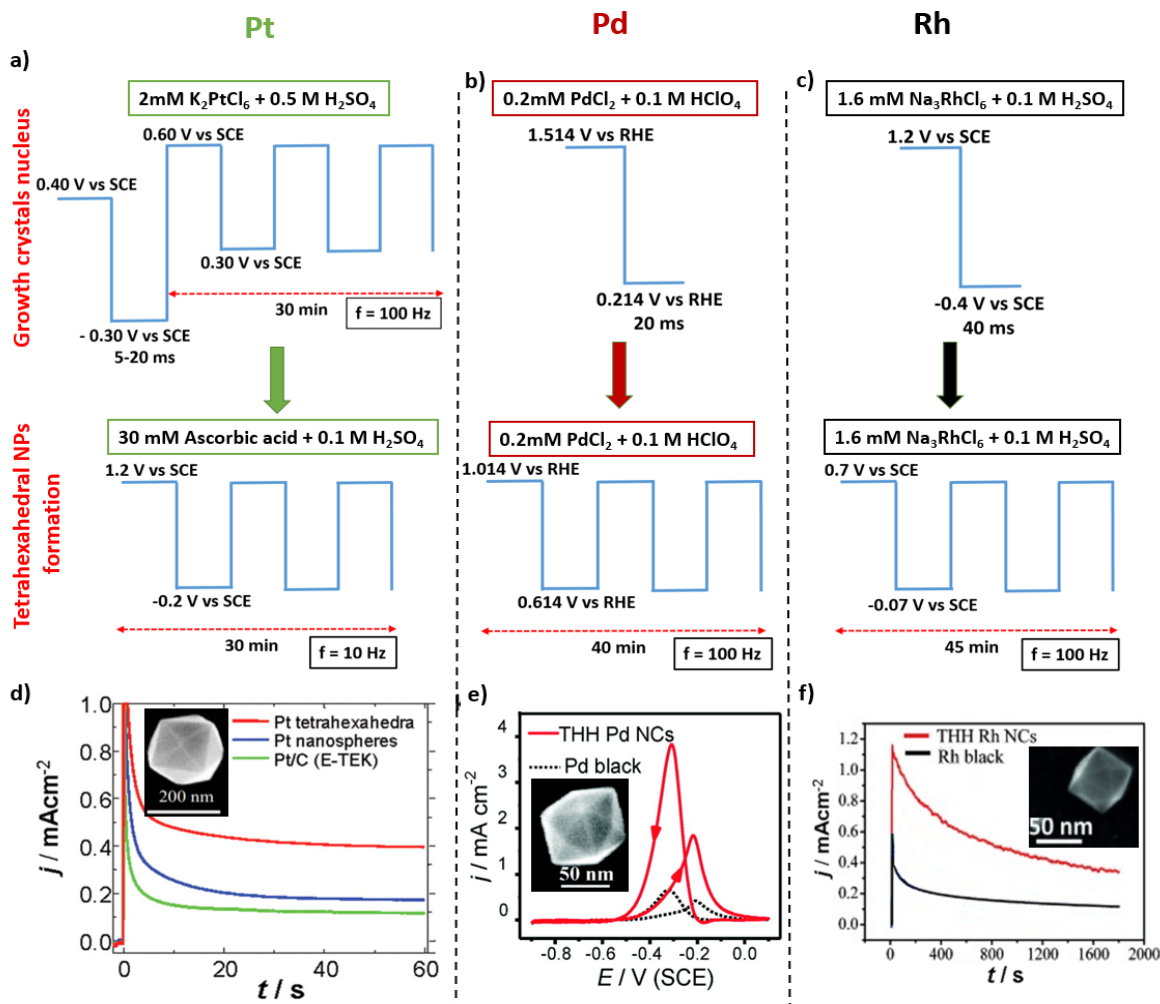
Figure 4. (a-c) Procedure for growing Pt (a), Pd (b) and Rh (c) tetrahexahedral NPs on a glassy carbon substrate by using electrochemical methods. (d) Transient current density curves at 0.55 V vs RHE for the Pt THH NPs (red), Pt nanospheres (blue), and Pt/C catalyst (green) in 0.1 M CH_3CH_2OH + 0.1 M $HClO_4$ solution (e) Cyclic voltammograms of THH Pd NPs (red solid line) and Pd black catalyst (black dashed line) at 10 mV s^{-1} in 0.1 M CH_3CH_2OH + 0.1 M NaOH (f) Current–time curves for THH Rh NPs (red) and Rh black catalyst (black) at 0.55 V vs RHE in 1.0 M CH_3CH_2OH +1.0 M NaOH solution. Reproduced with permission from ref. 42. Copyright 2007 Science (a,d), from ref 39. Copyright 2010 American Chemical Society (b,e), and from ref 41. Copyright 2014 Wiley (c,f).

In the second step, the development of the noble metal nuclei into shape-controlled NPs takes place. This stage is normally achieved by applying a square-wave potential method (Figure 4a-c). At the upper limit potential, the metal nucleus can be oxidized and partially dissolved to form the corresponding metallic ions. Then, these ions diffuse to the glassy carbon surface and are reduced to metallic atoms at the lower potential. By the periodical repetition of this process, the new well-controlled high-index facets nanocrystals grow by a nucleation and growth process on the glassy carbon surface, while the dissolution of the initial metallic nucleus occurs. Surprisingly, only high-index facet NPs have been possible to synthesize by the use of this square-wave potential treatment.

Tian et al., attributed this fact to the lower coordination number on high-index planes compared to low-index planes[42]. When lower is the coordination number more difficult is for the oxygen atoms to adsorb on the surface sites and instead, these atoms preferentially diffuse into the noble metal surface by the replacement of a metallic atom by an oxygen atom. By reducing the metal at the lower potential step these displaced atoms cannot recover the initial position. However, on high-index facets like {730} or {210} facets, the coordination number is lower and the oxygen atoms only adsorb on the stepped atoms taking place the exchange between oxygen and metallic atoms (Figure 5).
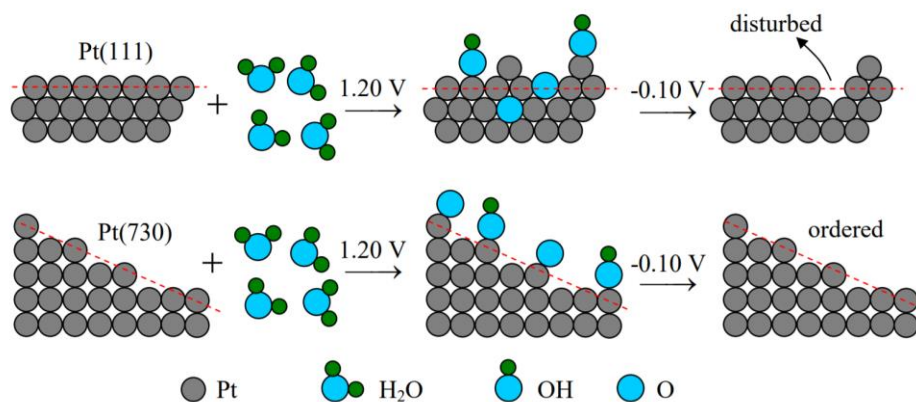

Figure 5. Schematic illustration of the different effect of oxygen adsorption/desorption on the surface structure of (111) and (730) of Pt. Reproduced with permission from ref. 42. Copyright 2007 Science

In general, an improved activity for EOR is expected for high-index faceted nanocrystals with a high density of low-coordinated atoms based on single crystals and DFT studies described in section 1. In this sense, the reactivity of noble-metals THH NPs has been studied toward the EOR by comparing their specific activities (catalytic activities normalized per active surface area) with the specific activities for non-shape controlled catalysts of the equivalent metal (commercial catalysts or synthesized noble metal nanospheres). In all cases, high-index THH NPs showed much higher specific activities than unshaped NPs, regardless of the noble metal employed as a catalyst (Figure 4 d-f). For example, Tian et al. found an enhanced (230 % of that on the nanospheres and 330% of that on the Pt/C) catalytic activity for equivalent Pt surface areas for EOR[42]. However, it is worthy to point out that the size of these high-index crystals synthesized by electrochemical methods is big (bigger than 50 nm), which results in a low noble metal utilization (much higher when compared to the unshaped commercial catalysts Pt THH and Pt/ETEK NPs). Therefore, the comparison of not only specific activities but also mass activities (currents normalized by the weight of the noble metal) is essential but, unfortunately, is missed in most of these works.

Besides that, theoretical simulations made by using Pt as a reference noble metal, have also demonstrated the superior reactivity for many chemical reactions on high-index faceted nanocrystals. More specifically, they demonstrated that tetrahexahedron enclosed by {310} facets possess the strongest tendency to form or break atomic bonds among the atomic arrangements of different surfaces[43]. However, although much research has been devoted to the synthesis of THH NPs, other shapes as concave Pt nanocubes[44], Pd nanorods[45], Pt triambic icosahedrons[46] and concave Pt THH NPs[47], have been also obtained by the electrochemical approach , showing a higher specific activity than that obtained on unshaped NPs of the equivalent metal (Figure 6).
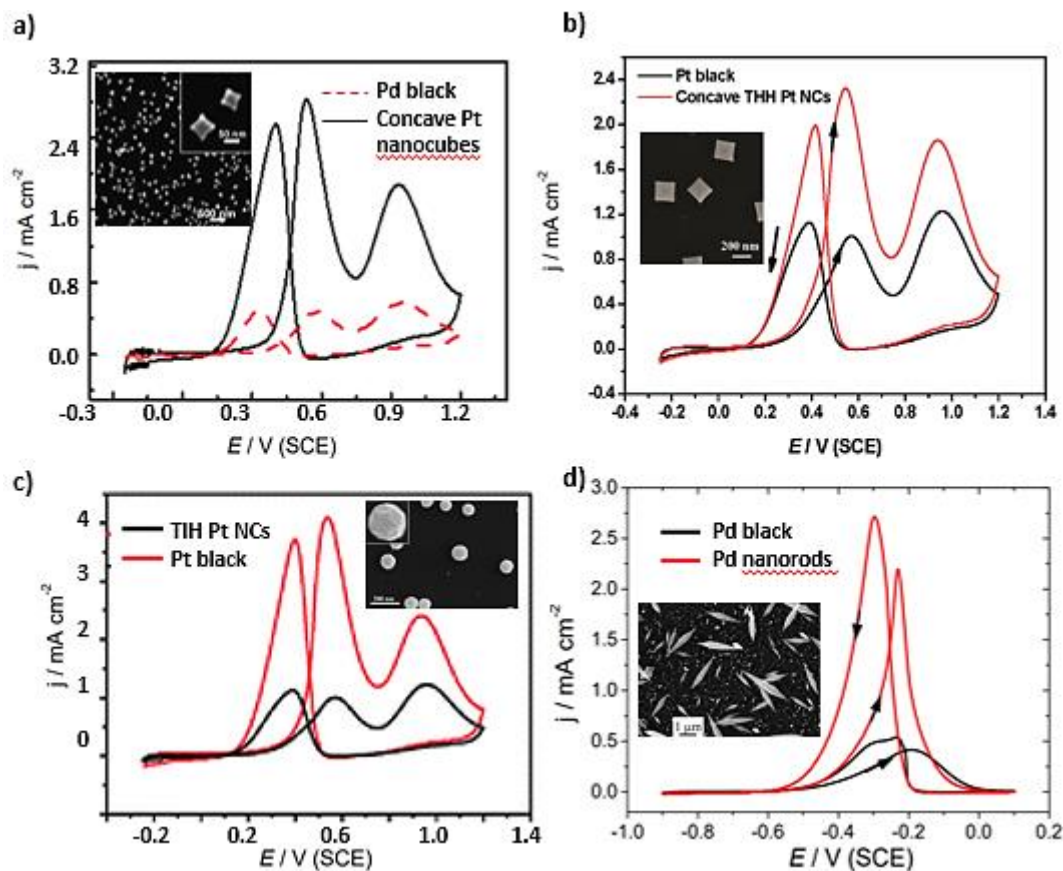

Figure 6. Comparison of the cyclic voltammograms for (a) concave Pt nanocubes (b) concave tetrahexahedral nanocubes (c) Pd nanorods and (d) tetraicosahedral Pt NPs with unshaped nanoparticles of the equivalent metal in 0.1 M EtOH + 0.1 M HClO₄ solution at 50 mV/s for (a-c) and 0.1 M EtOH + 0.1 M NaOH solution at 10 mV/s for (d). Reproduced with permission from ref. 44. Copyright 2016 Royal Society of Chemistry (a), from ref 47. Copyright 2009 Royal Society of Chemistry (b) from ref 46. Copyright 2013 Royal Society of Chemistry (c), and from ref 45. Copyright 2014 American Chemical Society (d)

Surprisingly, only pure noble catalysts have been synthesized by using this method for the EOR. As mentioned in the introduction section, the combination of noble metals with transition metals is a good strategy for increasing the activity/cost ratio of the catalytic material. However, to the best of our knowledge, no shape-controlled noble-

based materials have been synthesized by using electrochemical methods. Only one work can be find on the decoration of as-prepared THH Pt NPs with electrochemical methods by Bi adatoms[48]. In this work, a significant enhancement of the EOR was reported by increasing the coverage of Bi, being 0.68 the optimum coverage value.

2.2 Chemical synthesis

Whereas only the synthesis of monometallic high-index facets NPs has been reported by using electrochemical methods, by the use of chemical methods have been reported also the synthesis of not only high-index but also low-index monometallic, bimetallic and trimetallic NPs, such as cubic, octahedral and rhombic dodecahedral NPs with predominantly {100}, {111} and {110} facets, respectively[49–59].

Regarding monometallic catalysts, Feliu and coworkers studied the ethanol oxidation in acid media on different shape-controlled platinum nanoparticles: (100) and (111) predominantly oriented Pt nanoparticles with a preferential cubic and octahedron shape, respectively [50]. FTIRS and differential electrochemical mass spectrometry (DEMS) studies demonstrated that the C-C bond breaking was more favored on cubic Pt NPs (2B in Scheme 1), in agreement with the aforementioned results with Pt single crystals. On the other hand, cubic NPs showed a lower onset potential and higher currents for the EOR than the NPs with a significant fraction of (111) facets, which is explained by the low overpotential for OH adsorption on (100) domains and is again in agreement with previous works with single crystal electrodes [20].

Motivated by the great activity of cubic Pt NPs and that a second transition metal can enhance the oxidation of poisoning intermediate species such as CO formed from the C-C bond breaking, many groups have focused their research on the synthesis of bimetallic and trimetallic Pt-based cubic NPs for the EOR. For example, Pt has been combined with noble metals in a one-pot solvothermal synthesis to obtain bimetallic Pt-Rh or Pt-Pd cubic NPs[58,59]. In general, higher currents and better performance have been achieved by using bimetallic nanocubes composed of two different noble metals when compared to unshaped Pt NPs. However, the catalyst cost of these noble metals is still very high (Rh is even more expensive than Pt). With the challenge to build cheaper and more electrocatalytic efficient catalyst but also exposing highly-active Pt {100} facets on the surface, we recently synthesized Pt-Sn cubic core-shells for the EOR[52]. When the difference in the redox potential of the different metals that compose the catalyst is high, the metal ions with a higher reduction potential are reduced first and then serve as seeds for the successive reduction of a shell composed by the second metal ions, resulting in core-shell cubic nanoparticles. After cycling, some of the Sn atoms are leached from the surface leading to the formation of a Pt skin of approximately 0.5 nm, which confers high stability and exceptional electrocatalytic performance, with specific currents three times higher than unshaped Pt−Sn catalysts and six times higher than cubic Pt NPs.

Besides the high activity found on cubic NPs, some authors have found an enhanced activity on Pt and Pd-based NPs containing high-index facets compared to NPs with predominantly low-index facets of the same metal (Figure 7)[60,61].
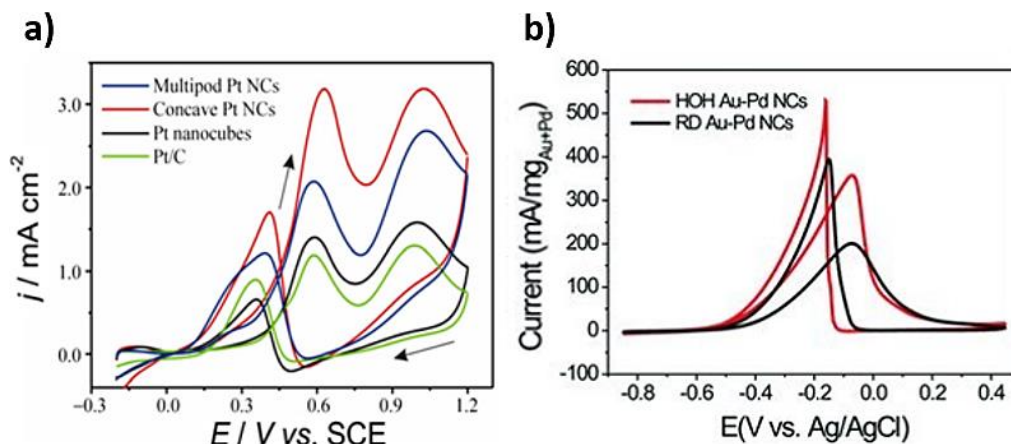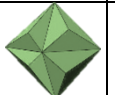

Figure 7. Cyclic voltammograms of (a) concave Pt nanocubes, multipod Pt NCs, Pt nanocubes and commercial Pt/C for EOR in 0.1 M EtOH + 0.1 M HClO$_4$ solution. Scan rate 50 mV/s (b) hexaoctahedral (HOH) and rhombic dodecahedral (RD) Au-Pd NPs in 0.1 M KOH + 0.5 M EtOH. Scan rate: 50 mV/s. Reproduced with permission from ref. 60. Copyright 2012 Springer (a), and from ref 61. Copyright 2013 Wiley (b).

This enhanced electroactivity is attributed to the high density of low-coordinated surface atoms with high surface energy in comparison with low-index facets. Although the synthesis of metal nanocrystals with high-index facets by chemical methods is not trivial because of their high surface energy, a few groups have been able to obtain NPs with such facets (Table 1).

Shape	Predominantly exposed facets	[a]Metallic precursors	[b]Surfactant	Reducing agent	Conditions	[c]Peak current (A/cm^2)	Ref.
Pt multipod	{211}	Pt(acac)$_2$	1-octylamine	1-octylamine	200 °C (3h)	~ 2.1	[60]
Pt concave nanocubes	{411}	Pt(acac)$_2$	1-octylamine formaldehyde	1-octylamine	200 °C (5h)	~ 3.2	[60]
Pt tetrahexahedrons	{310}	H$_2$PtCl$_6$		NaBH$_4$	Chemical reduction followed by square wave potential	[d]~ 1.1	[62]
Concave Pt polyhedral	{411}	H$_2$PtCl$_6$	PVP and methylamine	methylamine	160 °C (11h)	[d]~ 2.0	[63]
PtCuRh nanocages	{331}, {332}, {553}, {210}, {410}	HPtCl$_6$ RhCl$_3$ Cu(NO$_3$)$_2$	CTAB	Ascorbic Acid and oleylamine	160 °C (6h)	[e]7.3	[64]
Pd concave nanocubes	{100}, {730}, {310}	H$_2$PdCl$_4$	CTAC/CTAB	Ascorbic Acid		4.7	[65]
Au-Pd Rhombic dodecahedron	{110}	H$_2$PdCl$_4$ HAuCl$_4$	OTAC	Ascorbic Acid	60 °C (1h)	14.88	[66]
Au-Pd trisoctahedron	{221}	H$_2$PdCl$_4$ HAuCl$_4$	OTAC	Ascorbic Acid	60 °C (1h)	12.71	[66]
Au-Pd hexoctahedron	{421}	H$_2$PdCl$_4$ HAuCl$_4$	OTAC	Ascorbic Acid	60 °C (1h)	17.17	[66]
Pd-Au octapodal		NaAuBr$_4$ K$_2$PdCl$_4$	CTAC	Ascorbic Acid		2.2	[67]

[a] Pt(acac)$_2$ = platinum acetylacetonate; [b] CTAB = cetyltrimethyl ammonium bromide; CTAC = cetyltrimethyl ammonium chloride PVP = poly(vinylpirrolidone); OTAC = octadecyltrimethyl ammonium chloride [c]Currents normalized by the electrochemical surface area (ECSA), which was obtained based on the charge involved in the adsorption of hydrogen on the noble metal calculated by integrating the signals in the blank CVs without ethanol. These currents were recorded in 0.1 M ethanol solution at pH = 1 supporting electrolytes for Pt-based catalysts and pH = 13 for Pd-based catalysts. Scan rate = 50 mV s^{-1} [d] Scan rate = 10 mV s^{-1} [e] 0.5 M ethanol solution.

Table 1. Compilation of the different chemical synthesis methods for NPs with predominantly high-index facets for EOR and the peak current recorded in cyclic voltammograms during the EOR.

All of the aforementioned catalysts showed a high activity toward EOR with peak currents several times higher than that obtained on a commercial catalyst of the equivalent metal supported on carbon. One of the most interesting contributions was developed by Wang et al., who synthesized Pt-Cu-Rh nanocages containing abundant stepped atoms and various high-index facets around the surface[64]. Electrochemical tests showed that Pt–Cu–Rh HNCs exhibited an outstanding activity (peak current of 7300 A/cm^{-2}) attributed to the synergistic effect between Pt, Cu, and Rh components, its high specific surface area, as well as abundant concave/convex sites and the various high-index facets around the surface.

However, is not only essential to control the shape of the metallic NPs but also the morphology of the catalyst support, for the development of an optimum catalyst for the EOR[1]. An adequate catalyst supports should provide high electrical conductivity to favor electron transport and a large surface area to enhance the NPs dispersion. The anchoring of shape-controlled NPs on the catalyst support before the surfactant removal leads to a good dispersion of the NPs (even after the removal of the organic molecules), avoiding the NPs aggregation. Carbon blacks, like Vulcan XC-72R, are the most commonly employed materials as catalyst support[68]. However, in spite of the low cost and high availability of carbon blacks, they present a high amount of micropores, which results in diffusional problems and a limited NPs-anchoring. Additionally, the tolerance to corrosion of carbon blacks under the real fuel cell operating environment is low due to their amorphous structure[69]. However, by controlling catalyst support morphology, nature and nanostructure, it is possible to tune the size length and orientation of pores, as well as the external textural properties, which define the access and egress of ethanol and products through the whole material, respectively. Additionally, promoting or co-catalyst effects of nanostructured catalyst supports may enhance the EOR. Thus, the use of not only shape-controlled metal NPs but also tunable-morphology materials as a support for the catalytic material is also essential.

In the next section, we will briefly review and discuss recent advances on the synthesis of shape-controlled metal NPs supported on catalyst supports with a well-defined morphology for EOR. Despite the high variety of possible materials with well-controlled morphology to be used as catalyst support most of the works found in the literature only employ graphene oxide (GO) or reduced graphene oxide (RGO) and only a few works focus on different catalyst support with a well-defined structure.

2.3 Shape-controlled metal nanoparticles supported on tunable-morphology materials

As anticipated, the combination of shape-defined metal NPs and tunable-morphology supports represents a promising class of electrocatalysts for DEFCs.

In the carbon material family, graphene is a new membrane isolated for the first time in 2004 by Novaselov, Geim, and coworkers[70]. Graphene has a two-dimension (2D) and single-atom thick structure with sp^2

bonded carbon atoms arranged in a honeycomb-like lattice. It has a large theoretical surface area (about $2600 \text{ m}^2\text{g}^{-1}$)[71] and a fully conjugated sp^2 hybridized planar structure, resulting in an ultrahigh electrical conductivity ($105-106 \text{ Sm}^{-1}$)[72], excellent mechanical properties[73] and high thermoconductivity[74]. On the other hand, graphene oxide (GO) precursor contains a high density of surface functional groups (carbonyls, epoxides, hydroxyls, etc.) and lattice defects (vacancies, holes), which provide favorable sites for the anchoring and nucleation of metal NPs.[75–78]. This strong metal-graphene substrate interaction leads to improved durability of the supported-NPs. Additionally, graphene has a fast 2D electron-transfer kinetics resulting in enhanced activities for electrochemical reactions.[79] Due to all these unique chemical and physical properties, graphene nanosheets (GNs) have been used as 2D catalyst support in a wide range of applications, including the EOR[78].

During the last years, shape-controlled catalysts involving Pt and Pd supported on carbon GO or RGO have been synthesized for the EOR. More specifically, Pt and Pd-based cubic NPs with predominantly {100} supported on graphene have been reported[58,59,80,81]. These studies showed that, as compared to state-of-the-art commercial catalysts (Pt/C) or unsupported NPs of their equivalent metals, well shape-defined catalysts supported on this novel material exhibit higher catalytic performance and much higher durability for EOR.

Zhang et al. synthesized Pd nanocubes by a one-step synthesis approach involving the reduction of K_2PdCl_4 using ascorbic acid in the presence of KBr as capping agent[80]. Interestingly, this catalyst showed a maximum current density 4.29 times that of the unshaped Pd/RGO NPs and 2.64 times that of the unsupported Pd nanocubes.

However, bimetallic and trimetallic noble-metal cubic NPs supported on graphene have been shown more promising behavior than the aforementioned Pd nanocubes. For example, Zheng et al. synthesized Pt-Pd nanocubes with a size around 20.5 nm, and with Pt and Pd atoms uniformly distributed, indicating the formation of a PtPd alloy that was evidenced by EDS experiments (Figure 8a) and confirmed by XRD studies [58]. A great electrocatalytic behavior was found on this catalyst with a mass activity 60 times higher when compared to unshaped Pt NPs. This great activity could be explained by the presence of preferentially highly-active {100} Pt facets, as well as the modification of the Pt electronic structure by Pd via ligand effect, which results in a weaker binding energy of CO on Pt surface. An improvement in electroactivity has been also found on Pt-Rh nanocubes. Rao et al. synthesized Pt-Rh cubic NPs with different compositions and they found higher currents for all of them when compared to unshaped commercial Pt NPs (Figure 8b)[59]. Better performance for the C-C bond breaking from ethanol and its complete oxidation of CO_2 with the presence of Rh. They ascribed the electrocatalytic improvement to this specific shape as well as the synergistic effect of Pt and Rh.
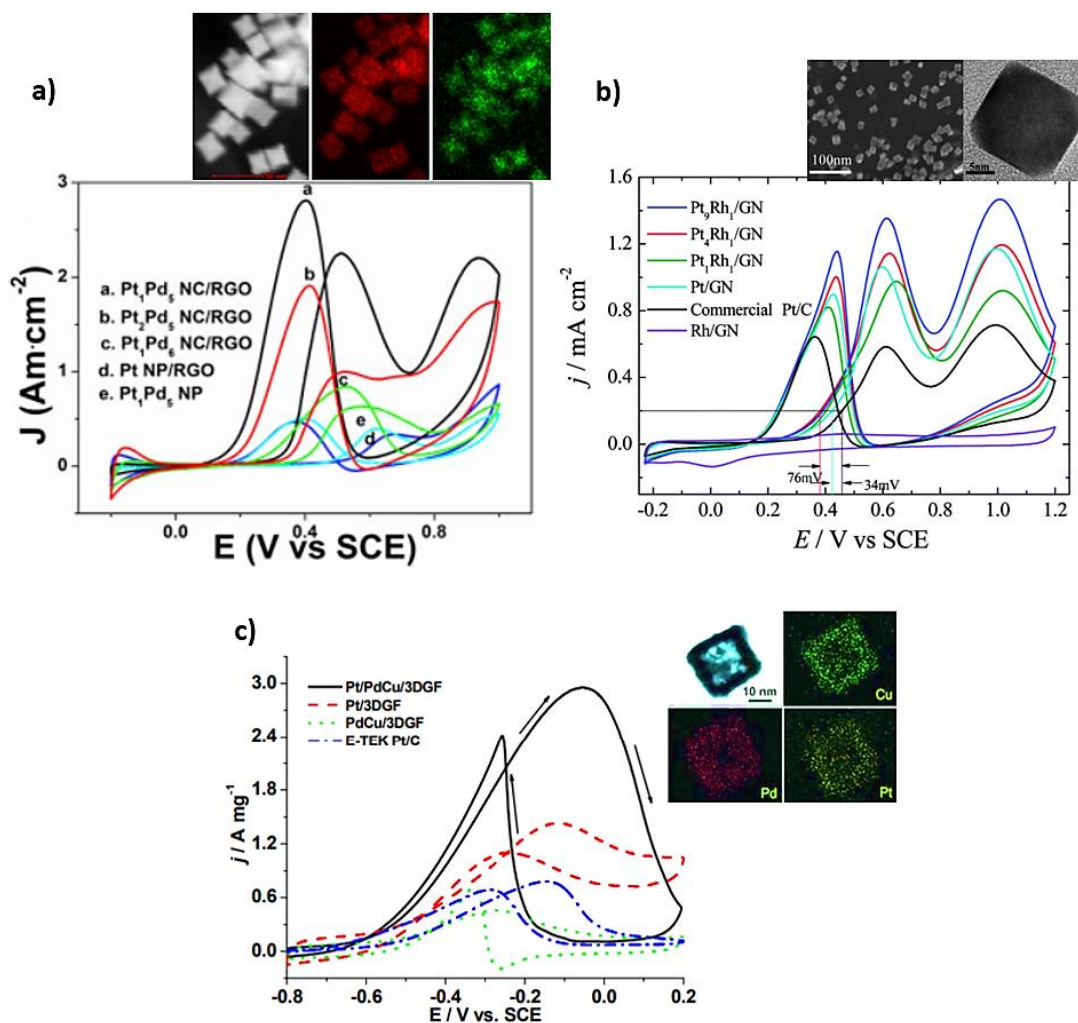
Figure 8. Cyclic voltammograms of (a) Pt and Pt-Pd cubic with different composition and unshaped Pt NPs supported on RGO and unsupported Pt-Pd NPs in 0.5 M CH_3CH_2OH + 0.5 M H_2SO_4 solution. Scan rate: 50 mV s^{-1} (b) Different atomic ratio Pt_xRh_y supported on graphene and commercial Pt/C in 0.1 M CH_3CH_2OH + 0.1 M $HClO_4$ solution. Scan rate 50 mV s^{-1} (c) Pt/PdCu, Pt, PdCu supported on 3D graphene and commercial 20% Pt/C catalysts in 1 M CH_3CH_2OH + 1 M KOH aqueous solution. Scan rate 50 mV/s. Reproduced with permission from ref. 58. Copyright 2018 Elsevier (a), from ref 59. Copyright 2014 Royal Chemistry Society (b), and from ref. 82. Copyright 2012 Wiley (c).

Furthermore, more complex shape-controlled trimetallic catalysts have been synthesized to be used in the EOR. In particular, a new ternary catalysts consisting on Pt/PdCu nanoboxes, with predominantly {100} facets anchored on a three-dimensional graphene framework (3DGF) were obtained by a dual solvothermal approach[82]. Authors found a superior activity for EOR on the ternary catalyst compared to Pt and PdCu electrodes, with a peak current around 3 times higher than those obtained on unshaped Pt/C and unshaped Pt/3DGF electrode and 6 times higher compared to the cubic PdCu/3DGF electrode, respectively (Figure

8c). Additionally, a higher durability was also obtained. This improved performance has been associated to synergic effects of the metals and the use of a 3D porous graphene structure, which facilitates the mass transfer and maximize the accessibility to the catalyst surfaces, as well as the cubic structure of the NPs. In our opinion, this work is of great relevance because of the incorporation of Cu in the cubic structure of the noble metals without perturbing the structure of the NPs, which allows not only higher activities but also a cheaper catalyst. However, although many authors have synthesized polycrystalline NPs with different shapes (nanoflowers, nanorings, nanodendrites, nanogarlands…)[83–92] to be used in the EOR, there are not works using metal NPs enclosed predominantly by high-index facets supported on materials with a well-defined nanoarchitecture.

In this regard, well-structured transition metal carbides and nitrides are paying attention in the last years[11,14,93]. These materials not only confer similar properties of carbon-based catalyst supports, but promoter (providing OH_{ad} species at smaller overpotentials than Pt) and co-catalyst (driving the reaction toward ethoxy pathway: 1 in Scheme 1) effects were also reported. Thus, higher energy conversion efficiency is expected.

Outlook

DEFCs are a promising technology for the generation of clean energy. Pt has been found to be the most active metal for the EOR. However, Pt is expensive, with low availability and it presents a low tolerance to intermediate-poisoning (mainly CO_{ad}). In order to address these issues, metal NPs dispersed on an appropriate support are generally used. These catalytic systems provide a higher metal utilization, enhancing the catalyst efficiency and reducing the catalyst cost. On the other hand, the EOR is well-known to be structure-sensitive and thus, the use of well-defined surfaces for the EOR seems to be a promising strategy for the development of electrocatalyts with superior activity. This review provides a perspective of the state-of-the-art for shape-controlled Pt catalysts for EOR.

Single crystal electrodes have been used to obtain fundamental knowledge on the activity of Pt crystal planes. However, the use of these electrodes in a commercial device is not possible. In order to design practical and efficient catalysts for the EOR, much research has been devoted to the synthesis of shape-controlled metal NPs with a predominant domain of the desired facet by electrochemical and chemical routes. As a summary, monometallic high-index noble metals crystals (Pt, Rh and Pd), mainly tetrahexahedral (THH) NPs, have been obtained by the electrochemical route. In contrast, the chemical method provides a higher versatility and it allows the growth of both high-index and low-index crystals (such as cubic, octahedral and rhombic dodecahedral with predominantly {100}, {111} and {110} facets,

respectively) of monometallic and bimetallic NPs. However, this last route usually requires the use of a surfactant to control NPs growth. The surfactant is strongly attached on the catalyst surface, blocking the active phase and consequently, a posterior surface clean treatment is required.

Regarding the performance of these catalysts, in general, a higher specific activity was obtained using well-defined NPs than those reported using non-shape controlled catalysts of the equivalent metal (commercial catalysts or synthesized nanospheres). In spite of these promising results, some challenges need to be solved in order to design well-defined surfaces as suitable catalysts for the EOR. Here, some specific directions are proposed to be considered in future studies:

i) Although significant efforts have been made in the use of monometallic and bimetallic noble metal NPs (such as Pt, Pd or Rh), the design of an efficient and cost-effective shape-controlled catalyst remains a key challenge. The combination of both Pt group metals and transition metals in bimetallic or trimetallic catalytic systems is a promising strategy to enhance the activity/cost ratio, which is the main limitation for the scaling-up of DEFCs. Besides to decrease the catalyst cost, the introduction of the transition metal may facilitate the removal of CO self-poisoning species by the generation of hydroxyl groups (bifunctional effect) or by modification of electronic properties (ligand effect). Consequently, high catalytic performance and durability may be anticipated in these shape-controlled catalysts. However, scarce works have been reported in the literature using chemical methods for the fabrication of well-defined surfaces involving transition metals, while the electrochemical approach has not been still explored (to the best of our knowledge).

ii) On the other hand, further research is still required in the synthesis of efficient NPs containing high-index facets (especially by the chemical approach). Higher activities have been reported using NPs with high-index factes when compared to cubic NPs of the same metal due to the higher density of low-coordinated surface atoms with a high surface energy of the former catalytic systems. In spite of these successful results, scarce works can be found in the literature involving the use of high-index crystal for the ethanol oxidation reaction.

iii) Besides to control the shape of metal NPs, the selection of a support with a suitable nanostructure is also essential. An ideal support should provide electrical conductivity to assure the electrical contact, a high specific surface area to enhance the dispersion of metal NPs and a developed mesoporosity to promote ethanol diffusion. The carbon black Vulcan is the conventional material used as a support for electrocatalytic applications. However, it presents a high micropore content and it undergoes electrooxidation during the EOR. In order to overcome these limitations, graphene has been used as a support of shape-controlled catalysts for the EOR obtaining promising results. In general, high performance and durability were reported, which was attributed to the strong metal-graphene interaction,

the high corrosion tolerance of graphene and the fast electron-transfer kinetics on this substrate. However, there is a lack of research in the use of other carbon materials or other susbtrates, such as electronically conductive polymers, metal oxides, carbides and nitrides, as support of shape-controlled NPs for the EOR. These materials offer different structural and chemical properties which could be optimized to enhance the performance in terms of activity and durability. Additionally, the use of well-defined nanoarchitectures with open and interconnected pores might facilitate the mass transfer and to maximize the ethanol accessibility to the active surfaces.

The increasing energy demand and the growing concern of global environmental resources has generated a world interest in promoting green and renewable energy sources. DEFCs are expected to play an important role in this sustainable energetic scenario. We hope that this review inspirer further research in the design of efficient, cost-effective and easily scaled-up shape-controlled catalysts for ethanol oxidation, making them more suitable to be used in DEFCs.

Present Addresses

Ruben Rizo, Department of Interface Science, Fritz-Haber Institute of the Max Planck Society, Faradayweg 4-6, 14195, Berlin, Germany.

Bibliographies

Dr. S. Pérez-Rodríguez received her B.Sc (2009) and Ph.D. (2015) in Chemical Engineering from the University of Zaragoza. She developed her Ph.D. on the electrochemical reduction of CO2 at Institute of Carbochemistry (Spanish National Research Council, CSIC). During this period, she enjoyed research stays at University of La Laguna and the Laboratory of Research in Fluid Dynamics and Combustion Technologies (CSIC). In 2016, she joined the Chemistry Technologic Centre of Catalonia (CTQC), where she worked on the design of nanocatalysts for electrochemical transformations of biomass-derived feedstocks. Currently, she is working as a Research Fellow at the University of Southampton (UK) under a project focused on lithium production and recycling. Her research interest includes the design of catalysts

for electrochemical applications and the development of energy-conversion devices, such as low temperature fuel cells and batteries.

Dr. Gonzalo García is a senior researcher (Viera y Clavijo Programme) at the University of La Laguna (Spain). He received his BSc in Chemistry from the National University of Córdoba (Argentina), subsequently he moved to Spain where he obtained his MSc and European PhD degree in Chemistry and Engineering Chemistry from the University of La Laguna (2007). He was involved in the photovoltaic/solar industry, as well as postdoctoral researcher at Leiden University (Netherlands) and at the Spanish National Research Council-ICP (Spain), before he moved to La Laguna in 2017. He was also a visiting researcher at the National University of Río Cuarto (Argentina), Sao Carlo Institute-USP (Brazil), University of the Republic (Uruguay), Pontifical Catholic University of Chile (Chile), Mannheim University of Applied Sciences (Germany), Consiglio Nazionale delle Ricerche-ITAE and University of Padova (Italy). His research interests are in fundamental and applied studies of electrochemical and electrocatalytic processes using a variety of conventional and non-conventional spectroelectrochemical techniques.

Dr. Rubén Rizo obtained his B.Sc. in Chemistry from the University of Alicante (Spain) in 2011 and his Ph.D. at the University of la Laguna in 2017. During his Ph.D. he was also a visiting researcher at the National University of Río Cuarto (Argentina), University of Cornell (USA), Carbochemistry Institute, CSIC (Spain) and University of Leiden (Netherlands). He is now a postdoctoral researcher in the Department of Interface Science at the Fritz-Haber Institute of the Max Planck Society (Berlin, Germany). His research interests include gaining fundamental insight on electrocatalytic processes based on single crystal work, as well as the synthesis, characterization, and electrocatalysis of shape-controlled metal nanoparticles.

References

[1]   R. Rizo, D. Sebastián, J. L. Rodríguez, M. J. Lázaro, E. Pastor, *J. Catal.* **2017**, *348*, 22–28.

[2]   L. García-Cruz, V. Montiel, J. Solla-Gullón, *Phys. Sci. Rev.* **2018,** *4*. doi:10.1515/psr-2017-0124.

[3]   S. Sun, M. C. Halseid, M. Heinen, Z. Jusys, R. J. Behm, *J. Power Sources* **2009**, *190*, 2–13.

[4]   N. Shakibi Nia, A. Martucci, G. Granozzi, G. García, E. Pastor, S. Penner, J. Bernardi, N. Alonso-Vante, J. Kunze-Liebhäuser, *Electrochim. Acta* **2019**, *304*, 80–86.

[5]   J. Flórez-Montaño, G. García, O. Guillén-Villafuerte, J. L. Rodríguez, G. A. Planes, E. Pastor, *Electrochim. Acta* **2016**, *209*, 121–131.

[6]   O. Guillén-Villafuerte, G. García, M. C. Arévalo, J. L. Rodríguez, E. Pastor, *Electrochem. commun.* **2016**, *63*, 48–51.

[7]   Divisek J. Low temperature fuel cells. In: Vielstich W, Lamm A, Gasteiger HA, Yokokawa H, editors. Handb. Fuel Cells, Wiley Online Library; 2010. doi:10.1002/9780470974001.f103008

[8]   M. Watanabe, H. Uchida, in *Handb. Fuel Cells-Fundamentals, Technol. Appl.* (Eds.: W. Vielstich, H. Yokokawa, H.A. Gastaiger), John Wiley & Sons Ltd, Chichester, **2010**, pp. 1–10.

[9]   W. Vielstich, A. Lamm, H. A. Gaseiger, *Handb. Fuel Cells—Fundamentals, Technol. Appl.* **2003**, *3*, 190.

[10]   R. I. Masel, R. I. Masel, *Principles of Adsorption and Reaction on Solid Surfaces*, John Wiley & Sons, **1996**.

[11]   G. García, O. Guillén-Villafuerte, J. L. Rodríguez, M. C. Arévalo, E. Pastor, *Int. J. Hydrogen Energy* **2016**.

[12]   M. Roca-Ayats, E. Herreros, G. García, M. A. Peña, M. V. Martínez-Huerta, *Appl. Catal. B Environ.* **2016**, *183*, 53–60.

[13]   M. Roca-Ayats, G. García, M. A. Peña, M. V. Martínez-Huerta, *J. Mater. Chem. A* **2014**, *2*, 18786–18790.

[14]   M. Roca-Ayats, O. Guillén-Villafuerte, G. García, M. Soler-Vicedo, E. Pastor, M. V. Martínez-Huerta, *Appl. Catal. B Environ.* **2018**, *237*, 382–391.

[15]   F. G. Will, *J. Electrochem. Soc.* **1965**, *112*, 451–455.

[16]   A. T. Hubbard, R. M. Ishikawa, J. Katekaru, *J. Electroanal. Chem. Interfacial Electrochem.* **1978**, *86*, 271–288.

[17]   K. Yamamoto, D. M. Kolb, R. Kötz, G. Lehmpfuhl, *J. Electroanal. Chem. Interfacial Electrochem.* **1979**, *96*, 233–239.

[18]   E. Yeager, W. E. O'Grady, M. Y. C. Woo, P. Hagans, *J. Electrochem. Soc.* **1978**, *125*, 348–349.

[19]   J. Clavilier, *J. Electroanal. Chem. Interfacial Electrochem.* **1980**, *107*, 211–216.

[20]   F. Colmati, G. Tremiliosi-Filho, E. R. Gonzalez, A. Berná, E. Herrero, J. M. Feliu, *Faraday Discuss.* **2009**, *140*, 379–397.

[21]   C. Busó-Rogero, E. Herrero, J. M. Feliu, *ChemPhysChem* **2014**, *15*, 2019–2028.

[22]   H.-F. Wang, Z.-P. Liu, *J. Am. Chem. Soc.* **2008**, *130*, 10996–11004.

[23]   G. García, M. T. M. Koper, *Chemphyschem* **2011**, *12*, 2064–72.

[24]   G. García, *ChemElectroChem* **2017**, *4*, 459–462.

[25]   C. Stoffelsma, P. Rodriguez, G. Garcia, N. Garcia-Araez, D. Strmcnik, N. M. Marković, M. T. M. Koper, *J. Am. Chem. Soc.* **2010**, *132*, 16127–16133.

[26]   F. Colmati, G. Tremiliosi-Filho, E. R. Gonzalez, A. Berna, E. Herrero, J. M. Feliu, *Phys. Chem. Chem. Phys.* **2009**, *11*, 9114–9123.

[27]   G. García, A. González-Orive, M. Roca-Ayats, O. Guillén-Villafuerte, G. Á. Planes, M. V. Martínez-Huerta, A. Hernández-Creus, E. Pastor, *Int. J. Hydrogen Energy* **2016**, *41*, 19674–19683.

[28]   S. C. S. Lai, M. T. M. Koper, *Phys. Chem. Chem. Phys.* **2009**, *11*, 10446–10456.

[29]   R. Rizo, M. J. Lázaro, E. Pastor, M. Koper, *ChemElectroChem* **2016**, *3*, 2196–2201.

[30]   V. Del Colle, A. Berna, G. Tremiliosi-Filho, E. Herrero, J. M. Feliu, *Phys. Chem. Chem. Phys.* **2008**, *10*, 3766–3773.

[31]   V. P. Santos, G. Tremiliosi-Filho, *J. Electroanal. Chem.* **2003**, *554*, 395–405.

[32]   L. Ma, D. Chu, R. Chen, *Int. J. Hydrogen Energy* **2012**, *37*, 11185–11194.

[33]   C. Xu, L. Cheng, P. Shen, Y. Liu, *Electrochem. commun.* **2007**, *9*, 997–1001.

[34]   E. D. Wang, J. B. Xu, T. S. Zhao, *J. Phys. Chem. C* **2010**, *114*, 10489–10497.

[35]   H. Angerstein-Kozlowska, B. MacDougall, B. E. Conway, *J. Electrochem. Soc.* **1973**, *120*, 756–

766.

[36]   M. Roca-Ayats, S. Pérez-Rodríguez, G. García, E. Pastor, in *Adv. Electrocatal. Low-Temperature Fuel Cells*, Springer, **2018**, pp. 51–89.

[37]   Y.-H. Chung, J. H. Jang, S. J. Kim, D. Y. Chung, H. Y. Park, I. Y. Cha, Y.-E. Sung, S. J. Yoo, H.-J. Kim, D. Henkensmeier, in *Meet. Abstr.*, The Electrochemical Society, **2015**, p. 1407.

[38]   M. Escudero-Escribano, G. J. Soldano, P. Quaino, M. E. Z. Michoff, E. P. M. Leiva, W. Schmickler, Á. Cuesta, *Electrochim. Acta* **2012**, *82*, 524–533.

[39]   N. Tian, Z.-Y. Zhou, N.-F. Yu, L.-Y. Wang, S.-G. Sun, *J. Am. Chem. Soc.* **2010**, *132*, 7580–7581.

[40]   Y. Qu, Y. Gao, L. Wang, J. Rao, G. Yin, *Chem. - A Eur. J.* **2016**, *22*, 193–198.

[41]   N. Yu, N. Tian, Z. Zhou, L. Huang, J. Xiao, Y. Wen, S. Sun, *Angew. Chemie Int. Ed.* **2014**, *53*, 5097–5101.

[42]   N. Tian, Z.-Y. Zhou, S.-G. Sun, Y. Ding, Z. L. Wang, *Science (80-.).* **2007**, *316*, 732–735.

[43]   R. Huang, Y.-H. Wen, Z.-Z. Zhu, S.-G. Sun, *J. Mater. Chem.* **2011**, *21*, 11578–11584.

[44]   B.-A. Lu, J.-H. Du, T. Sheng, N. Tian, J. Xiao, L. Liu, B.-B. Xu, Z.-Y. Zhou, S.-G. Sun, *Nanoscale* **2016**, *8*, 11559–11564.

[45]   N. Tian, Z.-Y. Zhou, S.-G. Sun, *Chem. Commun.* **2009**, 1502–1504.

[46]   L. Wei, Z.-Y. Zhou, S.-P. Chen, C.-D. Xu, D. Su, M. E. Schuster, S.-G. Sun, *Chem. Commun.* **2013**, *49*, 11152–11154.

[47]   L. Wei, Y.-J. Fan, N. Tian, Z.-Y. Zhou, X.-Q. Zhao, B.-W. Mao, S.-G. Sun, *J. Phys. Chem. C* **2011**, *116*, 2040–2044.

[48]   P. Wang, X. Lin, B. Yang, J.-M. Jin, C. Hardacre, N.-F. Yu, S.-G. Sun, W.-F. Lin, *Electrochim. Acta* **2015**, *162*, 290–299.

[49]   Z.-Y. Zhou, S.-J. Shang, N. Tian, B.-H. Wu, N.-F. Zheng, B.-B. Xu, C. Chen, H.-H. Wang, D.-M. Xiang, S.-G. Sun, *Electrochem. commun.* **2012**, *22*, 61–64.

[50]   C. Busó-Rogero, S. Brimaud, J. Solla-Gullon, F. J. Vidal-Iglesias, E. Herrero, R. J. Behm, J. M. Feliu, *J. Electroanal. Chem.* **2016**, *763*, 116–124.

[51]   C. Busó-Rogero, J. Solla-Gullón, F. J. Vidal-Iglesias, E. Herrero, J. M. Feliu, *J. Solid State Electrochem.* **2016**, *20*, 1095–1106.

[52]   R. Rizo, R. M. Arán-Ais, E. Padgett, D. A. Muller, M. J. Lázaro, J. Solla-Gullón, J. M. Feliu, E.

Pastor, H. D. Abruña, *J. Am. Chem. Soc.* **2018**, *140*, 3791–3797.

[53] R. M. Antoniassi, J. C. M. Silva, A. O. Neto, E. V Spinacé, *Appl. Catal. B Environ.* **2017**, *218*, 91–100.

[54] N. Erini, V. Beermann, M. Gocyla, M. Gliech, M. Heggen, R. E. Dunin-Borkowski, P. Strasser, *Angew. Chemie* **2017**, *129*, 6633–6638.

[55] P. Liu, Z. Cheng, L. Ma, M. Zhang, Y. Qiu, M. Chen, F. Cheng, *RSC Adv.* **2016**, *6*, 76684–76690.

[56] B. T. Sneed, C. N. Brodsky, C.-H. Kuo, L. K. Lamontagne, Y. Jiang, Y. Wang, F. Tao, W. Huang, C.-K. Tsung, *J. Am. Chem. Soc.* **2013**, *135*, 14691–14700.

[57] J. E. Sulaiman, S. Zhu, Z. Xing, Q. Chang, M. Shao, *ACS Catal.* **2017**, *7*, 5134–5141.

[58] Y. Zheng, J. Qiao, J. Yuan, J. Shen, A. Wang, S. Huang, *Int. J. Hydrogen Energy* **2018**, *43*, 4902–4911.

[59] L. Rao, Y.-X. Jiang, B.-W. Zhang, Y.-R. Cai, S.-G. Sun, *Phys. Chem. Chem. Phys.* **2014**, *16*, 13662–13671.

[60] L. Zhang, D. Chen, Z. Jiang, J. Zhang, S. Xie, Q. Kuang, Z. Xie, L. Zheng, *Nano Res.* **2012**, *5*, 181–189.

[61] Y. W. Lee, D. Kim, J. W. Hong, S. W. Kang, S. B. Lee, S. W. Han, *Small* **2013**, *9*, 660–665.

[62] S. Liu, N. Tian, A.-Y. Xie, J.-H. Du, J. Xiao, L. Liu, H.-Y. Sun, Z.-Y. Cheng, Z.-Y. Zhou, S.-G. Sun, *J. Am. Chem. Soc.* **2016**, *138*, 5753–5756.

[63] X. Huang, Z. Zhao, J. Fan, Y. Tan, N. Zheng, *J. Am. Chem. Soc.* **2011**, *133*, 4718–4721.

[64] K. Wang, H. Du, R. Sriphathoorat, P. K. Shen, *Adv. Mater.* **2018**, *30*, 1804074.

[65] J. Zhang, L. Zhang, S. Xie, Q. Kuang, X. Han, Z. Xie, L. Zheng, *Chem. Eur. J.* **2011**, *17*, 9915–9919.

[66] J. Zhang, C. Hou, H. Huang, L. Zhang, Z. Jiang, G. Chen, Y. Jia, Q. Kuang, Z. Xie, L. Zheng, *Small* **2013**, *9*, 538–544.

[67] J. W. Hong, Y. W. Lee, M. Kim, S. W. Kang, S. W. Han, *Chem. Commun.* **2011**, *47*, 2553–2555.

[68] S. Pérez-Rodríguez, E. Pastor, M. J. Lázaro, *Int. J. Hydrogen Energy* **2018**, *43*, 7911–7922.

[69] S. Pérez-Rodríguez, D. Sebastián, M. J. Lázaro, E. Pastor, *J. Catal.* **2017**, *355*, 156–166.

[70] K. S. Novoselov, A. K. Geim, S. V Morozov, D. Jiang, Y. Zhang, S. V Dubonos, I. V Grigorieva,

A. A. Firsov, *Science (80-.).* **2004**, *306*, 666–669.

[71]   K. M. Fair, X. Y. Cui, L. Li, C. C. Shieh, R. K. Zheng, Z. W. Liu, B. Delley, M. J. Ford, S. P. Ringer, C. Stampfl, *Phys. Rev. B* **2013**, *87*, 14102.

[72]   J. C. Ng, C. Y. Tan, B. H. Ong, A. Matsuda, *Procedia Eng.* **2017**, *184*, 587–594.

[73]   C. Lee, X. Wei, J. W. Kysar, J. Hone, *Science* **2008**, *321*, 385–8.

[74]   A. A. Balandin, *Nat. Mater.* **2011**, *10*, 569–581.

[75]   G. Arteaga, L. Rivera-Gavidia, S. Martínez, R. Rizo, E. Pastor, G. García, *Surfaces* **2019**, *2*, 16–31.

[76]   C. Xu, X. Wang, J. Zhu, *J. Phys. Chem. C* **2008**, *112*, 19841–19845.

[77]   R. Kou, Y. Shao, D. Mei, Z. Nie, D. Wang, C. Wang, V. V Viswanathan, S. Park, I. A. Aksay, Y. Lin, et al., *J. Am. Chem. Soc.* **2011**, *133*, 2541–2547.

[78]   M. Liu, R. Zhang, W. Chen, *Chem. Rev.* **2014**, *114*, 5117–5160.

[79]   M. Velický, D. F. Bradley, A. J. Cooper, E. W. Hill, I. A. Kinloch, A. Mishchenko, K. S. Novoselov, H. V. Patten, P. S. Toth, A. T. Valota, et al., *ACS Nano* **2014**, *8*, 10089–10100.

[80]   Y. Zhang, Q. Huang, G. Chang, Z. Zhang, T. Xia, H. Shu, Y. He, *J. Power Sources* **2015**, *280*, 422–429.

[81]   F. Zhu, K. Tu, L. Huang, X. Qu, J. Zhang, H. Liao, Z. Zhou, Y. Jiang, S. Sun, *Electrochim. Acta* **2018**, *292*, 208–216.

[82]   C. Hu, H. Cheng, Y. Zhao, Y. Hu, Y. Liu, L. Dai, L. Qu, *Adv. Mater.* **2012**, *24*, 5493–5498.

[83]   X. Chen, Z. Cai, X. Chen, M. Oyama, *J. Mater. Chem. A* **2014**, *2*, 315–320.

[84]   J.-J. Lv, N. Wisitruangsakul, J.-J. Feng, J. Luo, K.-M. Fang, A.-J. Wang, *Electrochim. Acta* **2015**, *160*, 100–107.

[85]   S.-S. Li, J.-J. Lv, L.-N. Teng, A.-J. Wang, J.-R. Chen, J.-J. Feng, *ACS Appl. Mater. Interfaces* **2014**, *6*, 10549–10555.

[86]   S.-S. Li, J.-N. Zheng, X. Ma, Y.-Y. Hu, A.-J. Wang, J.-R. Chen, J.-J. Feng, *Nanoscale* **2014**, *6*, 5708–5713.

[87]   G. Zhang, Z. Yang, W. Zhang, H. Hu, C. Wang, C. Huang, Y. Wang, *Nanoscale* **2016**, *8*, 3075–3084.

[88]   J. Zhang, A. Feng, J. Bai, Z. Tan, W. Shao, Y. Yang, W. Hong, Z. Xiao, *Nanoscale Res. Lett.* **2017**,

12, 521.

[89] Y. Tao, A. Dandapat, L. Chen, Y. Huang, Y. Sasson, Z. Lin, J. Zhang, L. Guo, T. Chen, *Langmuir* **2016**, *32*, 8557–8564.

[90] Q.-L. Zhang, J.-N. Zheng, T.-Q. Xu, A.-J. Wang, J. Wei, J.-R. Chen, J.-J. Feng, *Electrochim. Acta* **2014**, *132*, 551–560.

[91] A. Wang, X. He, X. Lu, H. Xu, Y. Tong, G. Li, *Angew. Chemie Int. Ed.* **2015**, *54*, 3669–3673.

[92] M. Hasan, S. B. Newcomb, J. F. Rohan, K. M. Razeeb, *J. Power Sources* **2012**, *218*, 148–156.

[93] N. S. Nia, A. Martucci, G. Granozzi, G. García, E. Pastor, S. Penner, J. Bernardi, N. Alonso-Vante, J. Kunze-Liebhäuser, *Electrochim. Acta* **2019**, *304*, 80–86.